K-shell spectroscopy of Ar clusters

E. Rühl, C. Heinzel, A. P. Hitchcock,[a] H. Schmelz,[b] C. Reynaud,[b] and H. Baumgärtel
Institut für Physikalische und Theoretische Chemie, Freie Universität Berlin, Takustrasse 3, D-1000 Berlin 33, Germany

W. Drube and R. Frahm
Hamburger Synchrotronstrahlungslabor HASYLAB at DESY, Notkestrasse 85, D-2000, Hamburg, 25, Germany

(Received 29 December 1992; accepted 25 January 1993)

Total ion yield spectra of a supersonic beam of Ar clusters have been recorded in the Ar K-shell ($1s$) spectral region using synchrotron radiation. The spectrum of the cluster component of beams containing argon clusters of mean size $\bar{N} \approx 400$ atoms is similar to that of the x-ray absorption spectrum of solid Ar. Analysis of the Ar $1s$ extended x-ray absorption fine structure (EXAFS) indicates an average first shell Ar–Ar distance in the cluster similar to that of the solid, but there is an increased Debye–Waller (disorder/thermal motion) term as well as changes in the higher coordination shell signals.Time-of-flight mass spectra and photoion–photoion coincidence (PIPICO) spectra of argon cluster beams are reported and the charge separation mechanisms of multiply charged argon clusters are discussed. The results are compared to those from recent studies of the Ar $2p$ spectra of Ar clusters.

I. INTRODUCTION

Clusters are a state of matter intermediate between isolated gas phase species and the condensed phase. Spectroscopic studies of clusters can give valuable insight into the nature of bonding in condensed phases. Recently, we have used Ar $2p$ spectroscopy to study the structure (geometric and electronic) and photoionization dissociation dynamics of van der Waals bonded Ar clusters.[1–3] A detailed rationale for studying the core excitation and ionic decay of rare gas clusters, along with a brief survey of related photoionization and structural studies has been presented elsewhere.[3] Inner-shell spectroscopy has potential advantages for such studies since it is a localized probe, particularly the extended fine structure (EXAFS) component.

In this work we report the first results of a study of the Ar $1s$ (K-shell) excitation and ionic decay spectroscopy of supersonic beams of Ar clusters. This is a technically challenging extension of our previous work in the Ar $2p$ regime since the $1s$ absorption cross section is two orders of magnitude weaker than the Ar $2p$ cross section. To our knowledge, this is the first report of Ar $1s$ spectra of free Ar clusters. There have been previous studies of the K-shell spectra of confined Ar clusters in the form of microscopic high pressure bubbles produced by ion implantation into a solid.[4,5] The Ar $1s$ x-ray absorption spectrum of free atomic argon has been studied frequently.[6–11] In addition, total and partial (Ar^{m+}, $m=1$–6) ion yield spectra of atomic argon have been reported.[12] The Ar $1s$ near edge x-ray absorption spectrum of solid argon has been compared to that of gaseous argon.[8] In this work we compare the near edge and extended fine structure signal in the Ar $1s$ spectrum of a cluster beam with that from the extended range Ar $1s$ spectrum of solid argon reported by Malzfeldt *et al.*[13]

II. EXPERIMENT

The spectra were recorded using synchrotron radiation from the EXAFS II station at HASYLAB operating in dedicated mode at 4.5 GeV. The cluster beam was generated using a novel compact apparatus[1,2,14] in which argon is expanded through a 50 μm conical nozzle at stagnation pressures (p_0) up to 5 bar with nozzle temperatures (T_0) between -120 °C and 30 °C. The indicated average cluster size ($\bar{N}$) was deduced from the stagnation pressure and nozzle temperature according to literature correlations.[15,16] $\bar{N}$ for Ar can be varied between 1 and 750 with the setup.

The density of the cluster beam and the path length of the x rays in the beam combine to provide an estimated absorption of 10^{-3} to 10^{-4} absorption lengths. An x-ray beam size of (10×3) mm was used with a total intensity of about 3×10^{10} photons s^{-1} eV^{-1}. Less than a third of these photons are used since the molecular beam is only about 1 mm in diameter. Total ion yield (TIY) and total electron yield (TEY) spectra were recorded using a channeltron adjacent to the cluster beam. The photon energy scale was calibrated by setting the energy of the Ar $1s\rightarrow4p$ resonance in atomic argon to the literature value of 3203.54 eV.[10]

In the previous Ar $2p$ studies,[3] the TEY spectra were more intense and thus of superior quality than the TIY spectra. However the electron yield signal at the Ar $1s$ edge was so much weaker than that at the Ar $2p$ edge that it contained a significant amount of background signal which was not associated with cluster beam ionization. Since the background in the ion yield detection channel was essentially zero, the Ar $1s$ TIY were of higher quality than the Ar $1s$ TEY spectra and thus only TIY spectra are reported

[a]Permanent address: Dept. of Chemistry, McMaster University, Hamilton, Ontario Canada L8S-4M1.
[b]Permanent address: DSM/DRECAM, Centre d'Etudes de Saclay, 91191 Gif-sur-Yvette, France.

 0021-9606/93/096820-07$06.00

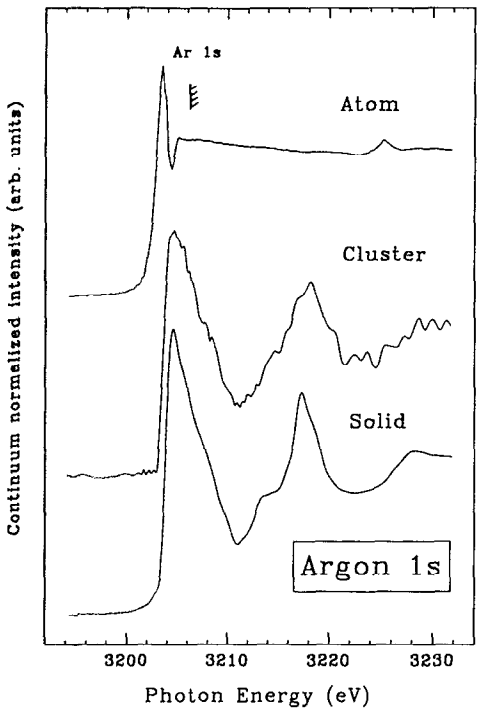

FIG. 1. Comparison of the near edge region of the total ion yield (TIY) Ar 1*s* spectrum of cluster argon (5 bar, -100 °C; $\bar{N}\sim400$) with the true absorption spectra of atomic (Ref. 11) and solid (Ref. 13) argon. The TIY cluster spectrum has had a $\simeq30\%$ contribution of atomic signal removed by subtraction of an appropriately scaled atomic spectrum. The data are continuum normalized and plotted on a common vertical scale. The absolute energy scale was set from the literature value (Ref. 10) for the atomic $1s\rightarrow4p$ transition.

here. Earlier Ar 2*p* studies[3] showed that TEY spectra are representative of the average beam composition whereas the TIY spectra are skewed toward the lower mass components of the cluster size distribution. As found in the Ar 2*p* studies, the Ar 1*s* TIY spectra always contained some contribution from the atomic signal. This has been subtracted from the as-recorded TIY spectrum, using the distinct low energy atomic $1s\rightarrow4p$ Rydberg signal to estimate the atomic fraction.

A time-of-flight mass spectrometer, with a pulsed extraction field as the time scale marker, was used to obtain mass spectra and partial ion yield (PIY) spectra. The square-wave ion extraction pulses were 0.6–1.5 μs wide and 300 V in amplitude. Photoion–photoion coincidence (PIPICO) and PIPICO-yield spectra were obtained using a continuous ion extraction field. The spectrum of the solid was recorded in transmission from a thin film of argon condensed on a thin Al window.[13]

III. RESULTS AND DISCUSSION

A. Near edge Ar 1s spectra

Figure 1 compares the Ar 1*s* total ion yield (TIY) spectrum of a highly clustered beam ($p_0=5$ bar, $T_0=-100$ °C, $\bar{N}=400$) with that of the atom[11] and that of the solid.[13] Under these cluster beam conditions there is a $\sim30\%$ atomic component[3] whose signal has been subtracted. The Ar_2^+ and Ar^+ partial ion yield spectra of the cluster beam, which should be specific to the cluster component, are similar in shape to the atom-corrected TIY spectrum, although they are considerably noisier because of the very low partial ion yields.

The Ar 1*s* spectrum of the atom is dominated by the strong $1s\rightarrow4p$ transition at 3203.5 eV. The Ar 1*s* spectrum of clustered argon is dramatically different. The threshold for Ar 1*s* absorption in clusters (evaluated as the midpoint of the leading edge) is 1.0 eV higher than in the atom. The full width at half maximum of the line corresponding to the Ar $1s\rightarrow4p$ Rydberg transition is only 0.8 eV, which is close to the estimated natural linewidth [0.7 eV full width at half-maximum (FWHM)[9]]. In the cluster this sharp atomic line is replaced by a broad, asymmetric peak (3–4 eV FWHM). The shape of the first feature in the argon cluster spectrum is similar to that of solid Ar (Fig. 1) suggesting that at this average cluster size ($\bar{N}=400$) the electronic properties have converged to those of the solid.[13] This was also the conclusion drawn from the similarity of the Ar 2*p* spectra of cluster beams with $\bar{N}>400$ and solid argon.[3] A part of the increased width of the first feature in the cluster spectrum is due to a smaller separation between the 4*p* transition (which increases in energy) and the Ar 1*s* ionization threshold (which decreases in energy). However, the increased width and the asymmetric line shape are associated primarily with the development of a conduction band in large clusters and solid argon.[17]

The 1.0(1) eV shift between the energy of the Ar $1s\rightarrow4p$ Rydberg transition in atomic argon (3203.5 eV) and the Ar $1s\rightarrow4p$ exciton in large cluster or solid argon (3204.5 eV) is identical to that of 1.0(1) eV observed between the (Ar $2p_{3/2}^{-1}$,4*s*) Rydberg state in Ar atom and the (Ar $2p_{3/2}^{-1}$,4*s*) exciton in large clusters[3] or solid Ar.[18] This suggests that at both edges the energy shift is mainly due to changes in the dielectric constant (or polarizability) between atom and cluster/solid. This would be reasonable if, in the region of the core orbital, the atomic Rydberg wave function and the cluster or condensed phase excitonic wave function have a similar spatial extent. This hypothesis is consistent with the observation of a near constant total intensity of the Ar $2p\rightarrow4s$ transitions as a function of cluster size.[3] Unfortunately, it is not possible to make a similar determination from the Ar 1*s* spectrum on account of the large overlap of the 4*p* exciton/conduction band and the ionization continuum in the cluster spectrum.

Above the 4*p* exciton peak there is a deep minimum followed by a maximum at 3218 eV. The ratio of the 4*p* maximum at 3210 eV in the corrected-TIY (and partial ion yield) spectra of the cluster beam is very similar to that in the absorption spectrum of solid Ar. This is further evidence that the corrected TIY spectrum is predominantly from the large cluster component of the molecular beam since contributions from the structureless atomic continuum would reduce the contrast of the peak at 3218 eV. In the Ar 2*p* spectrum of the solid and large clusters ($\bar{N}>400$) a number of narrow weak structures were observed which were attributed to longer range multiple scattering of the ionized photoelectron.[3] The shoulders at 3206 and

3208 eV and the peaks at 3214 and 3218 eV, which are clearly observed in the Ar 1*s* spectrum of solid argon, may have a similar origin. In the Ar 1*s* spectrum of atomic argon there are a number of prominent KM double excitation features around 3225 eV, which have been discussed in considerable depth recently.[11,19,20] KM double excitation features are not identifiable in the spectrum of either cluster or solid argon. This may be due to broadening of both the valence band excitations and the Ar $1s \rightarrow 4p$ transition which, in a sense, can be considered to be the components of these double excitation transitions. It is also possible the double excitation energies could differ substantially between the cluster/solid and the atom since the hole–hole Coulomb interaction should be reduced in larger systems. Future studies of the cluster size dependence of the KM double excitation region will be very interesting in this regard.

B. Ar 1*s* EXAFS of Ar clusters

Figure 2 compares the Ar 1*s* spectrum of cluster Ar with that of solid Ar[13] over an extended range. A linear background has been subtracted from the cluster spectrum in order to make its continuum slope match that of the measured spectrum of solid Ar, which is found to be a good match to calculated atomic cross sections.[21] The EXAFS signals from the solid and cluster have been isolated and converted to a wave number scale using standard EXAFS analysis techniques.[22] The magnitudes of the Fourier transforms of the EXAFS are presented in the insert to Fig. 2. Numerical results from the analysis (first-shell distances, coordination numbers, and Debye-Waller factors) are listed in Table I. Values derived from several choices of *k*- and *R*-space ranges are included to check for the stability of the results. Ar–Ar phase and amplitude functions calculated using the Feff spherical wave package[23] have been used in this analysis. The structural results for solid argon agree with the known values although the first shell Debye–Waller factor is somewhat larger than that deduced from an earlier analysis of the same data.[13] This difference could be related to the use of different calculated backscattering amplitude functions.[24]

While the average first shell distance and coordination number derived for the cluster beam and the solid are similar, the first-shell Debye–Waller term for the cluster is considerably larger than that for the solid. The increased Debye–Waller value could be caused by either static or dynamic disorder. Static disorder is expected since there must be a range of different sizes and geometries of clusters in the beam. higher coordination shell signal is detected in the Fourier transform of the Ar 1*s* EXAFS of the cluster beam, but it is much weaker and less well defined than in the solid (Fig. 2). The backscattering signal around 6.2 Å is extensively damped in the cluster relative to that in the solid. In solid argon this peak corresponds to the fourth coordination shell in the face centered cubic structure which has an enhanced intensity because of forward scattering in a three-atom collinear geometry. The strong damping of the corresponding component of the EXAFS signal of the argon cluster beam may be associated with the presence of a large bond angle distribution associated with static or dynamic disorder. This would be in line with recent theoretical work which predicts the existence of liquidlike structures in medium sized argon clusters ($\bar{N} \sim 100$).[25] Alternatively, it may be evidence for an icosahedral structure for clusters consisting of several hundred argon atoms, as has been proposed by electron diffraction studies of argon cluster beams.[16] In the icosahedral geometry the first and fourth shell are not collinear and thus there should not be any forward scattering intensity enhancement. Unfortunately, the limited statistical quality of the Ar 1*s* EXAFS spectrum so far obtained for cluster beams means that quantitative information concerning the higher coordination shells cannot be extracted reliably.

Figure 3 compares the Ar 1*s* and Ar 2*p* EXAFS $[k\chi(k)]$ of cluster argon. Both the experimental data (dashed line) and the Fourier filtered first shell signal (solid line) are presented. In addition, this figure compares the experimental results to the first shell components of the Ar 2*p* and Ar 1*s* EXAFS spectra calculated using the Feff spherical wave code.[23] The experimental and calculated EXAFS are in good agreement. There is a phase shift between the 1*s* and 2*p* EXAFS with a value between π and $\pi/2$, depending on the wave number. Early single scattering treatments of EXAFS predicted there should be a phase shift of π between *p* ionization and *s* ionization.[22,24] However, this neglects the differences in the central atom contribution to the total phase shift for *s* ($\Phi_a^{l=1}$) and *p* ($\Phi_a^{l=2}$, $\Phi_a^{l=0}$) ionization. This leads to systematic deviations from the simple prediction of a π phase shift (i.e., an inversion) between *s*- and *p*-shell EXAFS.[26]

The Ar 1*s* EXAFS spectrum of the clusters extends to larger wave number than that obtained at the Ar 2*p* edge. In principle, the larger *k* range of the Ar 1*s* data gives better *R*-space resolution which should allow extraction of more precise structural information. Ar 2*p* EXAFS is strictly limited to a k_{max} of 4.5 $Å^{-1}$ because of the onset of the Ar 2*s* edge. There is the additional complication of the spin–orbit splitting of the Ar 2*p* core hole state. The absence of these factors makes Ar 1*s* EXAFS preferable to Ar 2*p* EXAFS for structural analysis of argon clusters. Even the relatively limited precision Ar 1*s* EXAFS data obtained to date has given additional qualitative information about the higher coordination shell structure. When higher quality spectra are obtained, Ar 1*s* EXAFS will provide much more accurate information about average cluster structure than can ever be obtained from Ar 2*p* EXAFS studies.

C. Mass and PIPICO spectroscopy of Ar clusters

Figure 4 compares pulse-extraction time-of-flight photoionization mass spectra of atomic argon and the most highly clustered beam ($\bar{N}=400$) recorded with 3220 eV photon energy in the Ar 1*s* continuum. At this energy photoionization of atomic argon produces Ar^{4+} as the most abundant final charge state, along with considerable amounts of Ar^{3+} and Ar^{6+} and lesser amounts of Ar^{2+} and Ar^{7+}.[8,11] Auger-ion coincidence spectroscopy at the energy of the Ar $1s \rightarrow 4p$ Rydberg excitation[27] has shown that different electronic relaxation channels lead to differ-

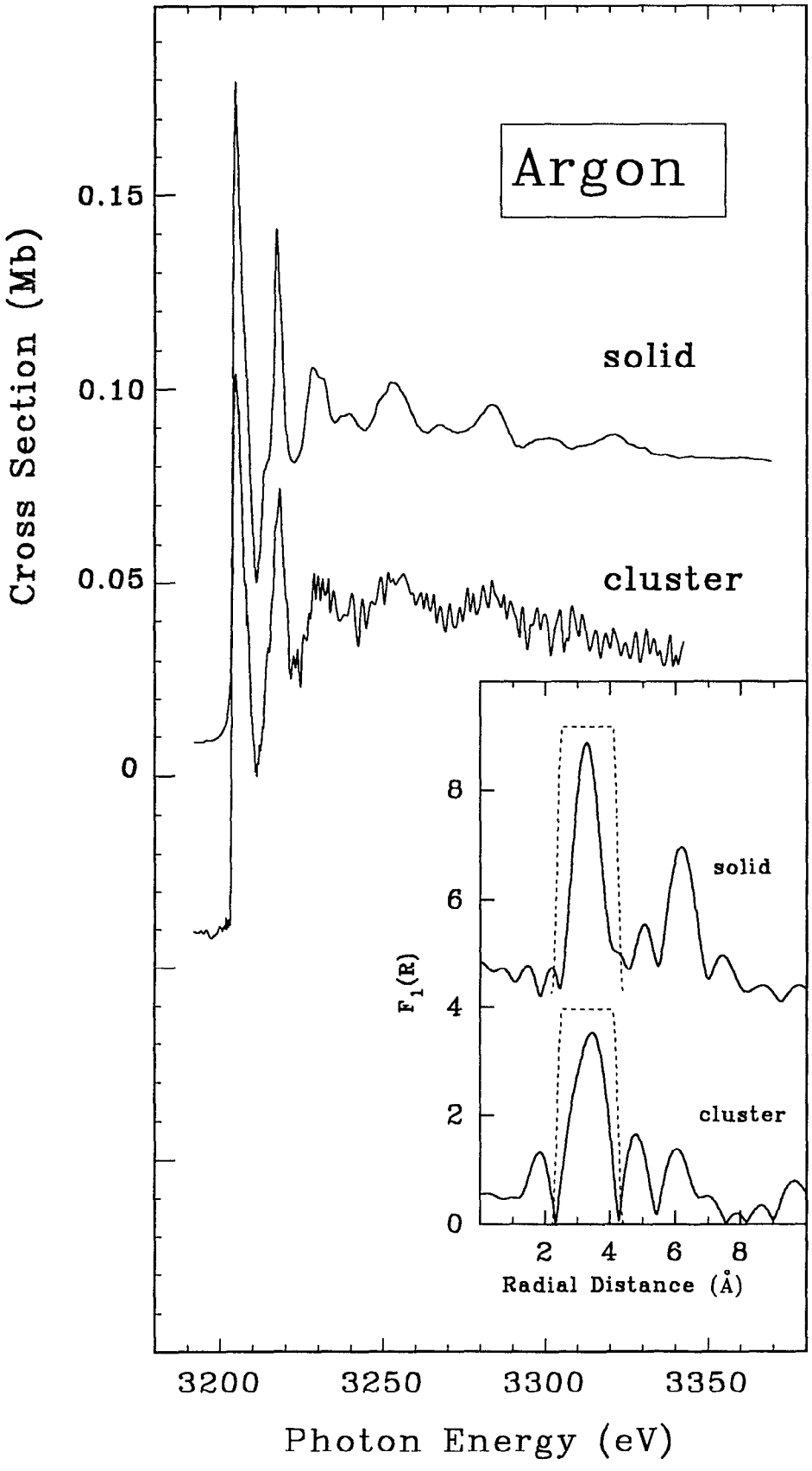

FIG. 2. Comparison of the extended range Ar 1*s* spectra of solid Ar (Ref. 3) and Ar clusters ($\bar{N}\sim400$). The absolute cross-section scale was set by matching the mean intensity of the continuum between 3240 and 3360 eV to that predicted for atomic argon (Ref. 2). The insert compares the magnitude of the Fourier transform using the k^1-weighted EXAFS data between 2.0 and 6.2 $Å^{-1}$ for both the Ar clusters and for solid Ar. The dashed line indicates the range of *R*-space data reverse transformed to obtain the Fourier filtered signal analyzed using calculated standards (Ref. 23) to obtain first shell structural information.

TABLE I. Distances (R), coordination numbers (N), and Debye–Waller factors ($\Delta\sigma^2$) derived from analysis of the Ar 1*s* EXAFS of solid and cluster argon.

Sample	Δk (Å^{-1})	ΔR (Å)	R (Å)	N	$10^{-3}\Delta\sigma^2$ (Å^2)
Solid[a]	1.3–8.8	2.0–5.4	3.76(2)	13(1)	26(3)
	2.1–8.8	2.2–4.6	3.75(1)	14(1)	28(2)
	2.0–6.2	2.2–4.4	3.76(1)	13(1)	22(3)
Previous analysis (Ref. 13)	2.0–9.0	2.0–4.2	3.76(1)	···	20(2)
Cluster[b]	1.1–6.2	2.0–5.4	3.86(10)	14(2)	36(8)
	2.0–6.2[c]	2.2–4.4[c]	3.82(2)	14(4)	54(8)

[a]Analysis of the Ar 1*s* EXAFS of a thin film of solid argon recorded in transmission (Ref. 13). Identical procedures (edge origin, background subtraction, k^1 weighting, apodization) were used in the analysis of the cluster and solid data. Δk and ΔR indicate the ranges of the data in wave number and distance space used in deriving the indicated results. Feff phase and amplitude standards (Ref. 23) computed for the first shell distance (3.755 Å) of solid argon were employed. A Debye–Waller term of zero is used in the calculation so the $\Delta\sigma^2$ values in the table are the mean square relative displacements associated with thermal motion and static disorder.

[b]An atomic component (amounting to about one third of the continuum intensity) was subtracted from the as-recorded TIY spectrum prior to this analysis.

[c]Conditions used for generating the Fourier transform (Fig. 2) and Fourier filtered first shell signal (Fig. 3).

ent highly charged atomic ions. KLM Auger decay yields mostly Ar^{3+} and Ar^{4+} whereas KLL Auger decay leads to more highly charged ions (from Ar^{3+} to Ar^{6+}). The efficient formation of highly charged ions in the Ar 1*s* regime is in sharp contrast to the Ar 2*p* regime where predominantly Ar^{2+} and Ar^{3+} are formed in LMM relaxation. The origin of these highly charged ions from Auger cascade and shake processes following K-shell ionization has been documented and discussed by Carlson and Krause[8] who have also noted the much higher average ion charge state following K-shell than L-shell ionization. Relative to their yields from Ti Kα ionization (4.97 keV),[8] we find a somewhat smaller proportion of Ar^{6+} (and more highly charged ions) in our spectrum recorded at 3220 eV. This is likely associated with the absence of KL and KM double excitation/ionization processes which have thresholds at 3226 and 3500 eV, well above the photon energy used.

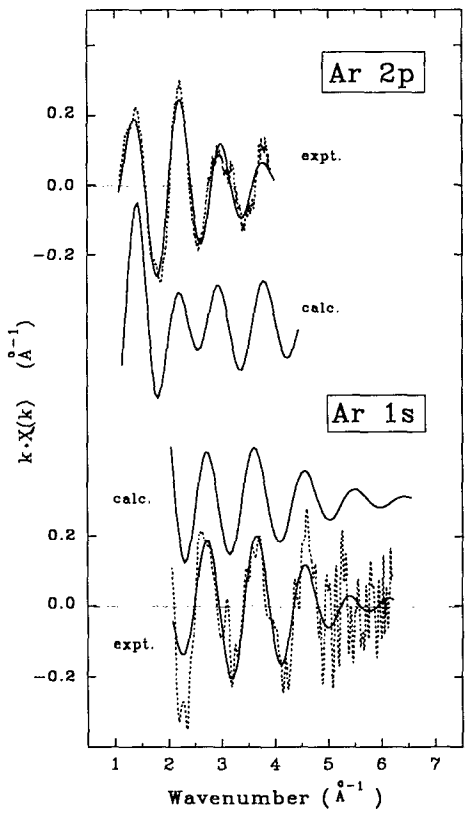

FIG. 3. Comparison of the Ar 2*p* (Ref. 3) and Ar 1*s* EXAFS of argon clusters ($\bar{N}\sim750$ for Ar 2*p*, $\bar{N}\sim400$ for Ar 1*s*) with that calculated by Feff (Ref. 23) for the Ar 2*p* and Ar 1*s* first shell EXAFS signal. The dashed line is the experimental data while the solid lines are the first shell component, Fourier filtered over $2.2<R<4.4$ Å using the Hanning apodization window indicated in Fig. 2.

In the mass spectrum of the argon cluster beam there is a weak signal from multiply charged atomic ions which is similar to that observed in the mass spectrum of atomic argon. This signal arises from the residual atomic component of the beam. The dominant signals from ionic fragmentation of the Ar 1*s* ionized clusters are the Ar_n^+ ($n=1,2,...$) ions. Clearly, cluster ionization and fragmentation does not generate multiply charged atomic ions. Interestingly, the overall shape of the photoionization mass spectrum of cluster argon is similar in the Ar 1*s* and Ar 2*p* regimes. The most intense mass spectral peak under beam conditions which produce large neutral clusters is the dimer cation (Ar_2^+). The Ar^+ and Ar_3^+ signals are also very strong in the cluster mass spectrum. Ar^+ arises almost exclusively from cluster fragmentation rather than from single ionization of the atomic component in the cluster beam.

Figure 5 shows the PIPICO spectrum of the $\bar{N}=400$ cluster beam recorded at 3220 eV. The only coincidences observed are those involving singly charged ions. This is the same result as found in earlier Ar 2*p* PIPICO studies.[2] The predominance of final states involving only singly charged ions is not surprising since only very large doubly ($n>91$) and triply charged ($n>226$) clusters are stable.[28]

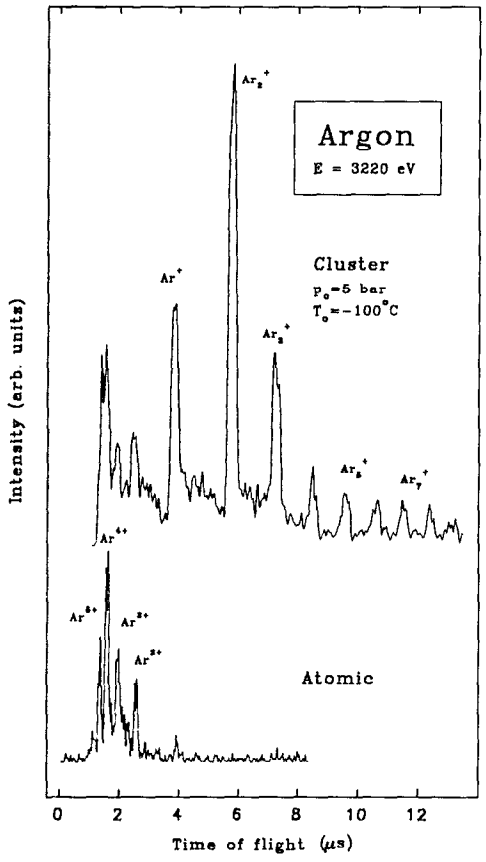

FIG. 4. Pulse time-of-flight mass spectra of atomic and cluster ($\bar{N}\sim400$) argon recorded with a photon energy of 3220 eV.

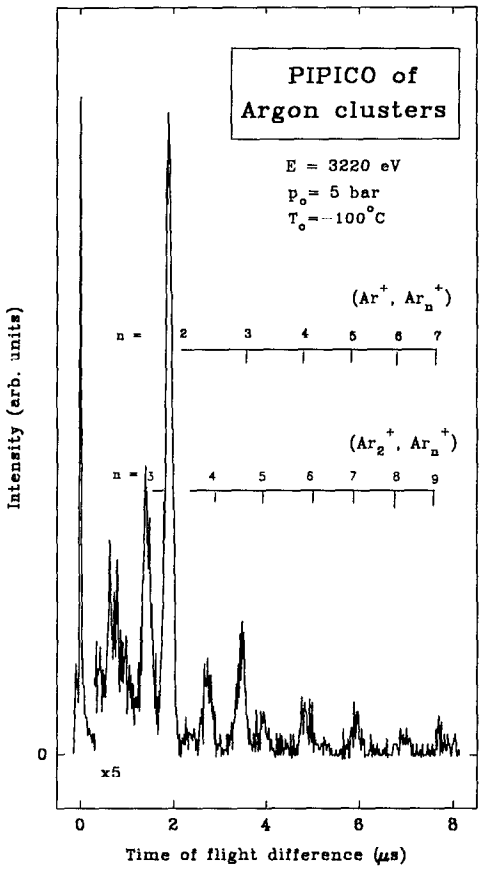

FIG. 5. PIPICO spectrum of argon clusters (p_0=5 bar, T_0=−100 °C; $\bar{N}\sim400$) recorded at 3220 eV photon energy. The ion pair assignments are based on mass spectra recorded under the same ion extraction and drift tube conditions.

However, we note that in the Ar 1*s* PIPICO the (Ar^+, Ar_2^+) signal is almost twice as intense as the (Ar_2^+, Ar_3^+) signal whereas these two ion pair signals have almost the same intensity in the Ar 2*p* PIPICO (compare Fig. 5 with Fig. 1 of Ref. 2). This is consistent with a higher average charge state from Ar 1*s* core hole decay and thus a greater extent of fragmentation in Ar 1*s* than in Ar 2*p* ionization of argon clusters.

The widths of the PIPICO signals are also found to be rather comparable to those in the Ar 2*p* PIPICO spectra. This shows that the maximum kinetic energy release is determined by electrostatic repulsion of positive charges in the clusters which is related to the Ar–Ar nearest neighbor distance.

The PIPICO spectrum can be divided into the region of symmetric charge separation ($\Delta t=0$) and that of asymmetric charge separation ($\Delta t>0$). The asymmetric charge separation channels consist of two series of ion pair signals. For one series the lighter ion is Ar^+ while for the other it is Ar_2^+. The predominance of asymmetric charge separation explains the large intensity of Ar^+ and Ar_2^+ in the cluster mass spectrum (Fig. 4). From Ar 1*s* ionization of the atom one expects that multiply ionized clusters (Ar_n^{3+}, Ar_n^{4+}, Ar_n^{5+}) are the initial product of core hole decay and electronic relaxation. This contrasts with Ar 2*p* excitation where mostly doubly charged clusters (Ar_n^{2+}) are formed initially. The general similarity of the PIPICO spectra of doubly charged and multiply charged clusters suggests that asymmetric charge separation dominates the decay for all degrees of ionization. After the loss of a singly charged Ar^+ or Ar_2^+ species, the remaining multiply charged cluster could then undergo sequential asymmetric charge separation to form small cluster fragments. These reactions are accompanied by losses of neutrals. This process has been studied in greater detail in a recent photoelectron–photoion–photoion (PEPIPICO) triple coincidence experiment in the Ar 2*p* regime.[29] As the average cluster size increases, charge separation in the Ar_m^{2+} cluster ion is followed by massive evaporation of neutrals. The Ar 1*s* and Ar 2*p* PIPICO spectra both show that highly charged atomic ions are not ejected intact in the charge separation process, but rather that singly charged ions are ejected. This suggests that the charge is dissipated over all of the cluster ion. Multiple coincidence experiments[30] are needed to deduce the complete mechanism of the fragmentation of multiply charged clusters.

IV. SUMMARY

This pioneering study has provided useful information on the Ar 1*s* spectroscopy of Ar clusters as well as considerable insight into the dominant mode of charge separation of highly charged clusters. The feasibility of using both the

near edge and extended fine structure aspects of the Ar 1*s* spectrum to characterize Ar clusters has been demonstrated. With increased flux in a smaller beam size, such as is available at modern wiggler or undulator beam lines, the signal strength could be improved by up to two orders of magnitude. An improvement in signal strength of this extent would allow acquisition of much higher quality spectra.

The cluster beam photoionization technique should also be extended to cluster species where the bonding in the condensed phase is very different from that in the atom. Examples would include aggregates of the metallic or semiconductor elements. These types of cluster studies would probably be more informative than studies of van der Waals clusters with regard to the evolution of bonding as a function of cluster size. X-ray absorption studies of metal–nonmetal transitions in clusters[31] would be of particular interest.

ACKNOWLEDGMENTS

Financial support by BMFT (Grant No. 05 5KEFXB5-TP3) is gratefully acknowledged. A.P.H. and E.R. acknowledge NATO for the support of a travel grant. We thank Dr. T. Tyliszczak for his generous assistance with the EXAFS analysis and for support of the analysis software (BAN—available from Tolmar Instruments, 397 E. 25th St., Hamilton, Ontario L8V 3A9, Canada).

[1] E. Rühl, H. W. Jochims, C. Schmale, E. Biller, A. P. Hitchcock, and H. Baumgärtel, Chem. Phys. Lett. **178**, 558 (1991).
[2] E. Rühl, H. W. Jochims, C. Schmale, E. Biller, M. Simon, and H. Baumgärtel, J. Chem. Phys. **95**, 6544 (1991).
[3] E. Rühl, C. Heinzel, A. P. Hitchcock, and H. Baumgärtel, J. Chem. Phys. **98**, 2653 (1993).
[4] Z. Tan, J. I. Budnick, D. M. Pease, and F. Namavar Phys. Rev. B **43**, 1987 (1991).
[5] G. Faraci, S. La Rosa, A. R. Pennisi, S. Mobilio, and G. Tourillon, Phys. Rev. B **43**, 9962 (1991).
[6] L. G. Parratt, Phys. Rev. **56**, 295 (1939).
[7] J. A. Soules and C. H. Shaw, Phys. Rev. **113**, 470 (1959).
[8] T. A. Carlson and M. O. Krause, Phys. Rev. **137**, 1655 (1965); T. A. Carlson, W. E. Hunt, and M. O. Krause, *ibid.* **151**, 41 (1966); M. O. Krause and T. A. Carlson, *ibid.* **158**, 18 (1967).
[9] M. O. Krause and J. H. Oliver, J. Phys. Chem. Ref. Data **8**, 329 (1974).
[10] M. Breinig, M. H. Chen, G. E. Ice, F. Parente, B. Crasemann, and G. S. Brown, Phys. Rev. A **22**, 520 (1980).
[11] R. D. Deslattes, Aust. J. Phys. **39**, 845 (1986).
[12] K. Ueda, E. Shigemasa, Y. Sato, A. Yagashita, M. Ukai, H. Maezawa, T. Hayaishi, and T. Sasaki, J. Phys. B **24**, 605 (1991).
[13] W. Malzfeldt, W. Niemann, P. Rabe, and R. Haensel, Springer Proceedings in Physics **2**, 445 (1984); W. Malzfeldt, Ph.D. thesis, University of Kiel, 1985.
[14] E. Rühl, C. Schmale, H. W. Jochims, E. Biller, R. Locht, A. P. Hitchcock, and H. Baumgärtel, *Particles and Fields Series 49, Synchrotron Radiation and Dynamic Phenomena,* AIP Conference Proceedings, edited by A. Beswick (AIP, New York, 1992), Vol. 258, p. 230.
[15] O. F. Hagena, Z. Phys. D **4**, 291 (1987); J. Wörmer, V. Guzielski, J. Stapelfeldt, G. Zimmerer, and T. Möller, Phys. Scr. **41**, 490 (1990).
[16] J. Farges, M. F. de Feraudy, B. Raoult, and G. Torchet, J. Chem. Phys. **78**, 5067 (1983); *ibid.* **84**, 3491 (1986).
[17] R. S. Knox and F. Bassani, Phys. Rev. **124**, 652 (1961).
[18] R. Haensel, N. Kosuch, U. Nielsen, U. Rössler, and B. Sonntag, Phys. Rev. B **7**, 1577 (1973).
[19] H. P. Saha, Phys. Rev. A **42**, 6507 (1990).
[20] M. Deutsch, N. Maskil, and W. Drube, Phys. Rev. A **46**, 3963 (1992).
[21] Optical Grapher Program. Available from M. Thomas, Centre for X-ray Optics, U.C. Berkeley.
[22] P. A. Lee, P. H. Citrin, P. Eisenberger, and B. M. Kincaid, Rev. Mod. Phys. **53**, 769 (1981).
[23] J. Mustre de Leon, Y. Yacoby, E. A. Stern, and J. J. Rehr, Phys. Rev. B **42**, 10843 (1990).
[24] B. K. Teo and P. A. Lee, J. Am. Chem. Soc. **101**, 2815 (1979).
[25] T. L. Beck, J. Jellinek, and R. S. Berry, J. Chem. Phys. **87**, 545 (1987); H. Matsuoka, T. Hirokawa, M. Satsui, and M. Doyama, Phys. Rev. Lett. **69**, 297 (1992).
[26] J. Chaboy, J. Garcia, and A. Marcelli, Solid State Commun. **82**, 939 (1992).
[27] J. C. Levin, C. Biedermann, N. Keller, L. Liljeby, C. S. O, R. T. Short, I. A. Sellin, and D. W. Lindle, Phys. Rev. Lett. **65**, 988 (1990); J. C. Levin, C. Biedermann, N. Keller, L. Liljeby, R. T. Short, I. A. Sellin, and D. W. Lindle, Nucl. Instrum. Methods B **56/57**, 124 (1991).
[28] P. Scheier and T. D. Mark, J. Chem. Phys. **186**, 3056 (1987); P. Scheier and T. D. Mark, Chem. Phys. Lett. **136**, 423 (1987).
[29] E. Rühl, C. Heinzel, P. Morin, M. Lavollée, and H. Baumgärtel, Z. Phys. D (to be submitted, 1993).
[30] J. H. D. Eland, F. S. Wort, P. Lablanquie, and I. Nenner, Z. Phys. D **4**, 31 (1986); J. H. D. Eland, Int. J. Mass Spectrom. **100**, 489 (1990); J. H. D. Eland, *Vacuum Ultraviolet Photoionization and Dissociation of Molecules and Clusters*, edited by C. Y. Ng (World Scientific, Singapore, 1991).
[31] R. E. Benfield, J. Chem. Soc. Faraday Trans. **88**, 1107 (1992).